Elastase I, FIBG, TS (mm), ATIII, Amylase, GLU. Table 1 gives an overview of the comparatively important fields that are utilised by the ILP to generate rules for Set Diff. Similarly, Table 2 summarises the highly ranked features for Set *N*1. Before applying the ILP algorithm to generate rules, we divide the data into three groups for these two data sets: 'low', 'normal' and 'high' groups. The criterion for classification is based on the definition of normal range provided by the National Cancer Center Hospital. For those values that are larger than the normal range, we denote them as the high group. Simultaneously, we classify the data into low group if its value is smaller than the normal range. For the purpose of illustration, we consider the normal range of FIBG is from 150 to 400 mg/dl. For data greater than 400 mg/dl, we classify it as the high group while we put those smaller than 150 mg/dl into the low group. The details for Set *N*1 can be found in Table 3. Similarly, we separate the data into several groups for Set Diff, and the details can be found in Table 4.

Each pancreatic record in the database represents an abnormality of a patient. A learning engine for proposing hypotheses (Aleph) ILP system has been proposed in [25]. Aleph adopts Muggleton's Progol algorithm for learning and generating rules from examples in [26]. In order to apply Aleph, all the data should be converted into Prolog facts. The conversion can be done in a straightforward and automatic way: each row in the database is translated into a number of Prolog facts.

Aleph aims to find one hypothesis H constructed by language L, such that: (i) H respects the constraints I; (ii) the $E+$ is derivable from (B and H) and (iii) the $E-$ is not derivable from (B and H). By default, Aleph uses a simple greedy set cover procedure that constructs such a hypothesis, one clause at a time. In the search for any single clause, Aleph selects the first uncovered positive example as the seed example, saturates this example and performs an admissible search over the space of rules that subsume the saturation, subject to a user-specified clause length bound [27]. Here, B corresponds to the features taken from the clinical data set. Positive examples are exactly represented by cases labelled as positive samples whereas negative examples are represented by cases labelled as negative samples. The algorithm works as follows: Initially, Aleph selects an example and searches the database for the facts known to be true about the specific example. Muggleton's insight [26] is that a combination of these facts should explain this example, and it should be possible to generalise that combination so that it will also explain other examples. The algorithm thus creates generalised combinations of the facts about an example, and searches for the combinations with the best performance. The performance of a rule depends on how well the rule covers (explains) positive examples and excludes negative examples. Once the ILP algorithms generate rules, one can judge whether they can reveal interesting and useful patterns.

Table 1 Important features conducted by the Aleph system for data Set Diff

Serum	Mass descriptors	Plasma
CA19-9	TS	FIBG
CEA	Location	—
GLU	—	—
Elastase I	—	—

The table illustrates the important fields selected by feature ranking for data Set Diff

Table 2 Highly ranked fields performed by Aleph system for data Set *N*1

Serum	Mass descriptors	Plasma
CA19-9	TS	FIBG
Amylase	—	ATIII
GLU	—	—
Elastase I	—	—

The table demonstrates the important fields selected by feature ranking in data Set *N*1

Table 3 Division of the selected features for Set *N*1

	Low	Normal	High
Elastase I	—	0–400 ng/dl	≥400 ng/dl
CA19-9	—	0–37 U/ml	≥37 U/ml
Amylase	≤42 IU/l	42–132 IU/l	≥132 IU/l
GLU	≤69 mg/dl	69–112 mg/dl	≥112 mg/dl
ATIII	≤80%	80–~140%	≥140%
FIBG	≤150 mg/dl	150–400 mg/dl	≥400 mg/dl

The table describes the classification of the normal, high and low groups. The criterion for the normal range is provided by the National Cancer Center Hospital. Subsequently, we can define the high and low groups, respectively

Table 4 Division of the top ranking features for Set Diff

	Low	Normal	High
Elastase I		0–400 ng/dl	≥400 ng/dl
CA19-9		0–37 U/ml	≥37 U/ml
GLU	≤69 mg/dl	69~112 mg/dl	≥112 mg/dl
CEA		0–5 ng/ml	≥5 ng/ml
FIBG	≤150 mg/dl	150–400 mg/dl	≥400 mg/dl

The table illustrates the criterion for classifying groups. The criterion is also provided by the National Cancer Center Hospital

3 Results

For the Set *N*1, we perform the ILP algorithm to generate a large amount of hypotheses, from which we select the rules with the best scores. We identify one potentially valuable hypothesis. The rule is given as follows:

Rule 1:
Patient A has positive lymph nodal metastasis if:

Patient A TS: large;
Patient A Elastase: normal, patient A AT: normal, patient A GLU: normal.

This rule states that if patient A is identified with

a) the mass:

- tumour is large

b) serum:

- Elastase I with the normal range

- GLU with the normal range

c) plasma:

- ATIII is in the normal range

then the lymph nodal metastasis is positive.

This hypothesis specifies 23 positive findings while misclassifying six negative findings as positive. The rule is useful as it identifies a close relationship between a malignant abnormality in a patient and the tumour size. Although the rule is obvious and a number of articles have been indicated that large tumour diameter is a strong predictor of the presence of the lymph nodal metastasis [6, 13, 28], it is still worth to mention that such result is obtained directly from the clinical laboratory data set. Therefore, it has been shown that ILP methods have successfully discovered the close relationship between the lymph nodal metastasis and the tumour size based on the clinical laboratory data set.

For the Set Diff, the ILP algorithm can also generate many rules. Among them, we identify two potentially interesting hypotheses. The rules are given below:

Rule 2:
Patient A has poorly differentiated tumour if:

Patient A CEA: high, patient A CA19-9: high, patient A FIBG: normal, patient A GLU: normal, patient A Location: ph.

This rule states that if patient A is identified with

a) the mass:

- tumour locates on the head of pancreas

b) serum:

- CA19-9 with the high level
- CEA with the high level
- GLU is in the normal range

c) plasma:

- FIBG is in the normal range

then the tumour is highly differentiated.

This rule covers 29 positive findings and four negative findings. This rule is valuable as it reveals the relationship between pancreatic cancer and CEA, CA19-9. To appreciate the significance of this rule, one should understand the characterisation of both CA19-9 and CEA, which implies that their glycobiological structures may play an important role in tumour differentiation. The fact that both CA19-9 and CEA are highly ranked among the features in Set Diff indicates the close relationship between differentiated pancreas cancers and glycobiological structures. A patient with high level CA19-9 and CEA is highly suggestive of malignancy. The level of serum CEA and CA19-9 in patients with pancreatic cancer were higher than that of other malignant diseases and benign pancreatic diseases [29]. CA19-9 has advantage in differential diagnosis between pancreatic cancer and chronic pancreatitis. This assists the assessment of treatment response, follow-up of pancreatic cancer and prognosis. Authors in [30] proposed that CA19-9 is a serum tumour marker that can assist in improving the survival rate if the patient could be identified earlier. Meanwhile, CEA plays an important role as marker in cancer research [31]. The detection of serum tumour markers is an effective and non-invasive diagnostic tool for pancreatic cancer. Thus, this rule performed by ILP has effectively revealed the serum tumour markers, which is extremely important since we can have much better therapeutic strategies for the pancreatic cancer patients.

Rule 3:

Patient A has poorly differentiated tumour if:
Patient A Elastase: high, patient A FIBG: normal, patient A CEA: high, patient A TS: large.

This rule states that if patient A is identified with

a) the mass:

- tumour is large

b) serum:

- CEA with the high level
- Elastase I with the high level

c) plasma:

- FIBG with the normal range

then the tumour is highly differentiated.

This rule identifies 19 positive findings whereas misclassifies two negative findings as positive. This rule is interesting as it discovers some determinants for pancreatic cancer. Elastase I is a serine protease which is an indirect test of pancreatic function. Thus, few studies investigated the role of Elastase I in pancreatic cancer. But in fact, high serum Elastase I could be a diagnostic clue to detect pancreatic cancer [32]. Authors in [33] have also reported that the CEA in the serum were significantly higher in patients with pancreatic carcinoma than in those with pancreatitis. Furthermore, the combination of the measurement of CEA and Elastase I in the serum is very useful for the detection of pancreatic carcinoma. This rule also further illustrates the tremendous potential of ILP technique in determining the determinants and facilitating the detection of the status of the lymph node metastasis and tumour differentiation.

4 Performance evaluation

We have developed a novel and simple approach to predict the pancreatic cancer status based on ILP technique. In this work, three rules are obtained by using the ILP technique based on the available data set. Each rule has specifically shown the relationship between the tumour differentiation or the lymph nodal metastasis and the related factors. In other words, one can find which feature(s) contribute(s) to the tumour differentiation or lymph nodal metastasis. The main idea of labelling the instances is that for those features of the instance which can satisfy the condition, we denote the corresponding instance as a positive sample. We also assume for those samples whose features are all within the normal range, we classify them as negative examples. This

doi: 10.1049/iet-syb.2013.0044

means for the ith instance in each rule, we define

$$\text{pregroundtruth}\ (i) = 1$$

if $f(x_{ik}) = v_k$, $k \in \{1, \ldots, m\}$ (m is the number of features in each rule) and $i \in \{1, \ldots, n\}$ (n is the number of instances). Here, v_k represents the value (low, normal or high) for the kth feature in the rule, x_{ik} represents the clinical value (a real number) of the kth feature for the ith instance and $f(x_{ik})$ is the value (low, normal or high) for the kth feature in the ith instance. Also, we define

$$\text{pregroundtruth}\ (i) = 0$$

if each $f(x_{ik})$ is in the normal range. Here, we use Rule 3 as an illustration. We can see that pregroundtruth = 1 when the Elastase I, FIBG and CEA of a patient are in the high, normal and high group, respectively, with the large tumour. If the above four features are all in the normal range, the pregroundtruth = 0. We let a_k, b_k, c_k to be the average value among high, normal and low ranges for the kth feature in a condition, respectively. Then, we further define $\tau(x)$ by

$$\tau(x_{ik}) = \begin{cases} a_k, & \text{for } x_{ik} \text{ in the high range group} \\ b_k, & \text{for } x_{ik} \text{ in the normal range group} \\ c_k, & \text{for } x_{ik} \text{ in the low range group} \end{cases}$$

For the other cases that fail to satisfy the above two conditions, we can also assign the label of the instance through comparing the distances, that is

$$\text{pregroundtruth}(i) = \begin{cases} 0, & \text{if } \sum\left(x_{ik} - \tau\left(x_{ik}\right)\right)^2 > \sum\left(x_{ik} - b_k\right)^2 \\ 1, & \text{otherwise} \end{cases}$$

The obtained pancreatic cancer files are then compared with the ground truth profile for performance evaluation. The accuracy of the learning performance is assessed as follows

$$\text{Accuracy} = \frac{\text{TP} + \text{TN}}{\text{TP} + \text{TN} + \text{FP} + \text{FN}}$$

Here, P is the true positive number, TN is the true negative number, FP is the false positive number and FN is the false negative number. We note that accuracy is exactly the ratio of the correctly predicted items to the whole number of data instances. In particular, we evaluate the above method by using a new data set (of size 174). We then conduct our proposed approach to the new data set and the results have shown that the accuracy for Rule 1 can be achieved by 83% which further confirms the effectiveness of our model. Although the results for Rules 2 and 3 are lower (68 and 71%, respectively), considering the difficulty of determining tumour differentiation, the fact that we could obtain over 70% and almost 70% accuracy even on such difficult samples shows promise that our proposed method may be effective when more data are accumulated. We also concern that whether our proposed model, as a classification method, can outperform the other methods. Therefore, we conduct a study on the comparison of our method with other classification methods. We select two well-known and popular classification methods for our comparisons.

4.1 Support vector machine (SVM)

A SVM constructs a hyperplane or set of hyperplanes in a high- or infinite-dimensional space, which can be used for classification. A good separation is achieved by the hyperplane that has the largest functional margin, that is, the distance to the nearest training data points of any class.

4.2 Decision tree

Decision tree learning is a method commonly applied in data mining. It employs a decision tree as a predictive model which maps observations about an instance to conclusion about the instance's target value. In the tree structures, leaves stand for classifications and branches represent conjunctions of features that lead to those classifications.

Cross-validation is a popular technique for assessing the generalisation ability of a statistical analysis. It holds the promise to evaluate the accuracy of a predictive model in practice. In particular, one round of cross-validation involves partitioning a sample of data into complementary subsets called training set and testing set, respectively. The training set is the one used for the analysis while the testing set is used for validation. Usually, multiple rounds of cross-validation are adopted with different partitions and the final validation result is obtained by taking the average over all the rounds. The performance of the classification model is measured through five-fold cross-validation, which means using a single observation from the original sample as the validation data while the remaining observations as the training data. Generally speaking, in each round, the original data are randomly divided into five subsamples. Among the five subsamples, a single subsample is retained as the validation data for testing the model. The remaining four subsamples are used as training data. The cross-validation process is then repeated five times (the folds), with each of the five subsamples used exactly once as the validation data. The average of the five results from the different fold is then used as a single estimation. Furthermore, we discuss the classification performance of our model by comparing with these two famous techniques. In particular, the results have shown that our method is superior to the other typical techniques in Table 5. Table 5 presents the accuracy comparison among the three approaches: SVM, decision tree and our proposed method. We can see that our method performs the best in both data sets. In particular, for Set $N1$, our proposed method can reach 83%, which evidently highlights the superiority of our method in fulfilling the task of prediction. In terms of Set Diff, our method performs relatively superior than the SVM and DT algorithms, reaching 68 and 71%, respectively, for Rule 2 and Rule 3. Thus, we can

Table 5 Accuracy comparison for the three methods

Data sets	Diff		$N1$
	Rule 2	Rule 3	Rule 1
PM	68%	71%	83%
SVM	57%	58%	—
DT	65%	67%	—

PM: proposed method; SVM: support vector machine; DT: decision tree

conclude that we have constructed a useful and effective framework to predict the patient status from the perspective of the classification performance.

ILP has distinct advantages over other data-mining techniques. It can facilitate the interaction between humans and computers by using background knowledge to narrow down the search space and return human-comprehensible results. Therefore it can take advantage of both the computer's speed and the human's knowledge. ILP technique has successfully identified important features for diagnosis and prognosis of pancreatic cancer. The first hypothesis has revealed that the tumour size is the strongest determinant of prognosis for pancreatic cancer, which is obtained by analysing the laboratory data. Although many advances can be seen in the fight against other cancers in recent years, the prognosis for patients diagnosed with the pancreatic cancer has remained extremely poor. The main reason is that the cancer is not suspected and is difficult to diagnose in its early stages, when most people are asymptomatic or have non-specific symptoms that are easily ignored or attributed to other diseases. Researchers have found a striking correlation between a patient's prognosis and the size of their tumour at the time of diagnosis. Unfortunately, relatively small number of the patients with small tumours have been correctly detected. We cannot find their tumours until they become comparatively large. Accordingly, most patients have advanced carcinoma at the time of diagnosis, which makes it impossible to resect the tumour curatively. One can have a much better chance of helping patients survive from pancreatic cancer if they can be identified relatively early and the tumour size is relatively small. Thus, the detection of the tumour size is not an efficient approach to cure pancreatic cancer and serum markers are needed for diagnosis or prognosis of pancreatic cancer. The second rule discovered by our experiment demonstrates that CEA antigen above the cutoff levels of 5.0 ng/ml and CA19-9 above the cutoff limit of 37 U/ml are highly predictive of malignancy. The final hypothesis discovers that a combination of measurements of CEA and Elastase I in the serum is very useful for the detection of pancreatic carcinoma. All the rules play a vital role in determining the tumour differentiation and the status of the lymph node metastasis. This illustrates the effectiveness of our proposed ILP method.

Furthermore, this study opens up the possibility for applying computational machine-learning techniques to clinical data. This shows that there is a huge and new resource, such as accumulated routine laboratory results, for the development of biomarkers and therapeutic design in cancer research. Moreover, this type of prediction can be applied to other diseases with appropriate data. We have shown that this accumulated clinical data makes it possible to predict the tumour differentiation and the status of lymph node metastasis contributing to the selection of therapeutic modalities. Our experiments also show that ILP techniques can identify valuable hypotheses. The clinical data provides an opportunity for data mining and ILP methods hold great promise to enable us to learn from laboratory data. As a result, we can improve the detection of carcinomas and the design of cancer therapeutics. Moreover, the rules obtained by ILP method provide us a platform to develop classification model to predict the status of patients. From the perspective of the classification accuracy, our proposed model outperforms the other typical machine-learning techniques.

5 Concluding remarks

In this paper, we utilise the ILP as a study model. Furthermore, to avoid the effects of uncertainties derived from various factors, we put our endpoint not on prediction of patient survival but on the histological background of the tumour. We utilise the laboratory data and employ the ILP methodology in our analysis. Our results indicate that ILP technique is an effective method to uncover the underlying characteristic of cancer that can benefit the cancer patient to attain better therapeutic strategies. Furthermore, we have developed a classification model based on ILP technique and the superiority of the model has been assured by the experimental results.

6 Acknowledgments

The authors would like to thank the three anonymous referees for their helpful and constructive suggestions. Research supported in part by GRF grant and HKU CERG grants, National Natural Science Foundation of China grant nos. 11271144 and S201201009985. We would also like to thank Karin Yokozawa for preparing the clinical data.

7 References

1 Yeo, C.J., Cameron, J.L., Lillemoe, K.D., *et al.*: 'Pancreaticoduodenectomy for cancer of the head of the pancreas. 201 patients', *Ann. Surg.*, 1995, **221**, (6), pp. 721–733
2 Matsuno, S., Egawa, S., Fukuyama, S., *et al.*: 'Pancreatic cancer registry in Japan: 20 years of experience', *Pancreas*, 2004, **28**, (3), pp. 219–230
3 Kuhlmann, K.F., de Castro, S.M., Wesseling, J.G., *et al.*: 'Surgical treatment of pancreatic adenocarcinoma; actual survival and prognostic factors in 343 patients', *Eur. J. Cancer*, 2004, **40**, (4), pp. 549–558
4 Biankin, A.V., Kench, J.G., Colvin, E.K., *et al.*: 'Expression of S100A2 calcium-binding protein predicts response to pancreatectomy for pancreatic cancer', *Gastroenterology*, 2009, **137**, (2), pp. 558–68
5 Wang, Y., Xia, X.Q., Jia, Z., *et al.*: 'In silico estimates of tissue components in surgical samples based on expression profiling data', *Cancer Res.*, 2010, **70**, (16), pp. 6448–6455
6 Lim, J.E., Chien, M.W., Earle, C.C.: 'Prognostic factors following curative resection for pancreatic adenocarcinoma: a population-based, linked database analysis of 396 patients', *Ann. Surg.*, 2003, **237**, (1), pp. 74–85
7 Maeshiro, K., Ikeda, S., Yasunami, Y., *et al.*: 'Long-term outcome of small pancreatic cancer carcinoma', *SyoukakiGazou*, 2006, **8**, (4), pp. 421–428
8 Adham, M., Jaeck, D., Le Borgne, J., *et al.*: 'Long-term survival (5-20 years) after pancreatectomy for pancreatic ductal adenocarcinoma: a series of 30 patients collected from 3 institutions', *Pancreas*, 2008, **37**, (4), pp. 352–357
9 Perini, M.V., Montagnini, A.L., Jukemura, J., *et al.*: 'Clinical and pathologic prognostic factors for curative resection for pancreatic cancer', *HPB(Oxford)*, 2008, **10**, (5), pp. 356–362
10 Chung, C.K., Zaino, R.J., Stryker, J.A.: 'Colorectal carcinoma: evaluation of histologic grade and factors influencing prognosis', *J. Surg. Oncol.*, 1982, **21**, (3), pp. 143–148
11 Berti Riboli, E., Secco, G.B., Lapertosa, G., *et al.*: 'Colorectal cancer: relationship of histological grading to disease prognosis', *Tumori*, 1983, **69**, (6), pp. 581–584
12 Tobita, K., Kijima, H., Dowaki, S., *et al.*: 'Thrombospondin-1 expression as a prognostic predictor of pancreatic ductal carcinoma', *Int. J. Oncol.*, 2002, **21**, (6), pp. 1189–1195
13 Yeo, C.J., Abrams, R.A., Grochow, L.B., *et al.*: 'Pancreaticoduodenectomy for pancreatic adenocarcinoma: postoperative adjuvant chemoradiation improves survival. A prospective, single-institution experience', *Ann. Surg.*, 1997, **225**, (5), pp. 621–633
14 Pawlik, T.M., Gleisner, A.L., Cameron, J.L., *et al.*: 'Prognostic relevance of lymph node ratio following pancreaticoduodenectomy for pancreatic cancer', *Surgery*, 2007, **141**, (5), pp. 610–618
15 Zacharias, T., Jaeck, D., Oussoultzoglou, E., *et al.*: 'Impact of lymph node involvement on long-term survival after R0

doi: 10.1049/iet-syb.2013.0044

pancreaticoduodenectomy for ductal adenocarcinoma of the pancreas', *J. Gastrointest. Surg.*, 2007, **11**, (3), pp. 350–356
16 Hattangadi, J.A., Hong, T.S., Yeap, B.Y., *et al.*: 'Results and patterns of failure in patients treated with adjuvant combined chemoradiation therapy for resected pancreatic adenocarcinoma', *Cancer*, 2009, **115**, (16), pp. 3640–3650
17 Katz, M.H., Wang, H., Fleming, J.B., *et al.*: 'Long-term survival after multidisciplinary management of resected pancreatic adenocarcinoma', *Ann. Surg. Oncol.*, 2009, **16**, (4), pp. 836–47
18 Lavrac, N., Dzeroski, S.: 'Inductive logic programming: techniques and applications' (Ellis Horwood, New York, 1994)
19 Sobin, L., Gospodarowicz, M., Wittekind, C.: 'TNM classification of malignant tumors' (Wiley, Hoboken, NJ, 2009, 7th edn.)
20 Hruban, R.H., Boffetta, P., Hiraoka, N., *et al.*: 'World Health Organization classification of tumours. Pathology & genetics', in: 'Tumours of the digestive system' (IARC Press, Lyon, 2010, 4th edn.)
21 Xuan, G.R., Chai, P.Q., Wu, M.H.: 'Bhattacharyya distance feature selection', *Pattern Recognit.*, 1996, **2**, pp. 195–199
22 Chen, X.W., Michael, W.: 'Fast: a roc-based feature selection metric for small samples and imbalanced data classification problems'. Proc. 14th ACM SIGKDD Int. Conf. Knowledge Discovery and Data Mining, 2008, pp. 124–132
23 Dash, M., Liu, H.: 'Feature selection for clustering'. Proc. PAKDD-00, 2000, pp. 110–121
24 Saeys, Y., Inza, I., Larranaga, P.: 'A review of feature selection techniques in bioinformatics', *Bioinformatics*, 2007, **23**, (19), pp. 2507–2517
25 Srinivasan, A.: 'The Aleph manual'. http://web.comlab.ox.ac.uk/oucl/research/areas/machlearn/Aleph/alephtoc.html, 2001
26 Muggleton, S.: 'Inverse entailment and Progol', *New Gener. Comput.*, 1995, **13**, pp. 245–286
27 Elizabeth, B.M.D., Davis, J., Costa, V.S., *et al.*: 'Knowledge discovery from structured mammography reports using inductive logic programming'. AMIA Annual Symp. Proc., 2005, pp. 96–100
28 Fortner, J.G., Klimstra, D.S., Senie, R.T., *et al.*: 'Tumor size is the primary prognosticator for pancreatic cancer after regional pancreatectomy', *Ann. Surg.*, 1996, **223**, (2), pp. 147–153
29 Ni, X.G., Bai, X.F., Mao, Y.F., *et al.*: 'The clinical value of serum CEA CA19-9 and Ca242 in the diagnosis and prognosis of pancreatic cancer', *Eur. J. Surg. Oncol.*, 2005, **31**, (2), pp. 164–169
30 Ruckert, F., Pilarsky, C., Crutzmann, R.: 'Serum tumor markers in pancreatic cancer-recent discoveries', *Cancers*, 2010, **2**, (2), pp. 1107–1124
31 Goldenbery, D.M., Neville, A.M., Carter, A.C., *et al.*: 'CEA (carcinoembryonic antigen): its role as a marker in the management of cancer', *J. Cancer Res. Clin. Oncol.*, 1981, **101**, (3), pp. 239–242
32 Hamano, H., Hayakawa, T., Kondo, T.: 'Serum immunoreactive Elastase in diagnosis of pancreatic diseases. A sensitive marker for pancreatic cancer', *Dig. Dis. Sci.*, 1987, **32**, (1), pp. 50–56
33 Tatsuta, M., Yamamura, H., Noguchi, S., *et al.*: 'Values of serum carcinoembryonic antigen and Elastase 1 in diagnosis of pancreatic carcinoma', *Gut*, 1984, **25**, (12), pp. 1347–1351

www.ietdl.org

SYBSI20130044

Author Queries

Yushan Qiu, Kazuaki Shimada, Nobuyoshi Hiraoka, Kensei Maeshiro, Wai-Ki Ching, Kiyoko F. Aoki-Kinoshita, Koh Furuta

Q1 Please provide editor names in ref. [20].

Carcinogenesis vol.35 no.8 pp.1840–1846, 2014
doi:10.1093/carcin/bgu112
Advance Access publication May 24, 2014

A human cancer xenograft model utilizing normal pancreatic duct epithelial cells conditionally transformed with defined oncogenes

Yuki Inagawa[1,2], Kenji Yamada[1], Takashi Yugawa[1], Shin-ichi Ohno[1], Nobuyoshi Hiraoka[3], Minoru Esaki[4], Tatsuhiro Shibata[5], Kazunori Aoki[6], Hideyuki Saya[2] and Tohru Kiyono[1,*]

[1]Division of Virology, National Cancer Center Research Institute, 5-1-1 Tsukiji, Chuo-ku, Tokyo 104-0045, Japan, [2]Division of Gene Regulation, Institute for Advanced Medical Research, School of Medicine, Keio University, 35 Shinanomachi, Shinjuku-ku, Tokyo 160-8582, Japan, [3]Division of Molecular Pathology, National Cancer Center Research Institute, 5-1-1 Tsukiji, Chuo-ku, Tokyo 104-0045, Japan, [4]Hepatobiliary and Pancreatic Surgery Division, National Cancer Center Hospital, 5-1-1 Tsukiji, Chuo-ku, Tokyo 104-0045, Japan and [5]Division of Cancer Genomics and [6]Division of Gene and Immune Medicine, National Cancer Center Research Institute, 5-1-1 Tsukiji, Chuo-ku, Tokyo 104-0045, Japan

*To whom correspondence should be addressed. Tel: +81 3 3547 5275; Fax: +81 3 3543 2181;
Email: tkiyono@ncc.go.jp

Pancreatic ductal adenocarcinomas (PDACs) are considered to arise through neoplastic transformation of human pancreatic duct epithelial cells (HPDECs). In order to evaluate the biological significance of genetic and epigenetic alterations in PDACs, we isolated primary HPDECs and established an *in vitro* carcinogenesis model. Firstly, lentivirus-mediated transduction of KRAS^{G12V}, MYC and human papillomavirus 16 (HPV16) E6/E7 under the control of a tetracyclin-inducible promoter efficiently immortalized and transformed primary HPDECs, which gave rise to adenocarcinomas subcutaneously in an immune-deficient mouse xenograft model, depending on expression of the four genes. The tumors regressed promptly upon shutting-off the oncogenes, and the remaining tissues showed histological features corresponding to normal ductal structures with simple columnar epithelium. Reexpression of the oncogenes resulted in development of multiple PDACs through pancreatic intraepithelial neoplasia-like structures. We also succeeded in efficient immortalization of primary HPDECs with transduction of mutant CDK4, cyclin D1 and TERT. The cells maintained a normal diploid status and formed duct-like structures in a three-dimensional culture. In combination with p53 silencing, KRAS^{G12V} alone was sufficient to fully transform the immortalized HPDECs, and MYC markedly accelerated the development of tumors. Our PDAC model supports critical roles of KRAS mutations, inactivation of the p53 and p16-pRB pathways, active telomerase and MYC expression in pancreatic carcinogenesis and thus recapitulates many features of human PDAC development. The present system with reversible control of oncogene expression enabled *de novo* development of PDAC from quasinormal human tissues preformed subcutaneously in mice and might be applicable to carcinogenesis models in many organ sites.

Introduction

Pancreatic ductal adenocarcinoma (PDAC) is one of the most lethal human cancers. It is characterized by late diagnosis due to lack of early symptoms, extensive metastasis and high resistance to chemotherapy and radiation. Despite advances in the clinical management of the disease, only ~6% of patients survive 5 years after diagnosis and prognosis of PDAC remains poor (1–4). Further work is needed to elucidate the events driving pancreatic carcinogenesis to have any hope of eventually conquering this disease.

Although the cells-of-origin for PDAC remain controversial, a multistep carcinogenesis process has become widely accepted. In this concept, PDAC arises from precursor lesions termed Pancreatic Intraepithelial Neoplasia (PanIN) involving multiple genetic alterations. Four genes, KRAS (>90%), p16/CDKN2A (>95%), p53 (50–75%) and DPC4/SMAD4 (55%) are found to be commonly mutated or inactivated in PDAC (1–3). These are classified as driver alterations for development of PDAC.

Genetically engineered mouse models of PDAC are excellent experimental systems which have helped to improve our understanding of the disease. In these models, invasive cancers that resemble human PDAC can be induced by combinations of two or three genetic alterations in precursors of mouse pancreas (5). However, there are biological differences between mice and humans. Since the altered expression of the genes is sufficient to produce metastatic cancers, limits exist as to the capacity to investigate new candidate cancer gene functions. Therefore, other approaches using human materials, such as human pancreatic cancer cell lines and human normal pancreatic cells, are also needed, in addition to the use of genetically engineered mouse models.

Recently, we have established *in vitro* multistep carcinogenesis models for cervical cancer, epithelial ovarian cancer and oral cancer (6–8). In the present study, taking advantage of this background, we could successfully immortalize and transform primary human pancreatic duct epithelial cells with defined genetic elements. Using a tetracyclin-inducible system, we found, for the first time, that bimodal expression of oncogenes brings out reversible features of transformation and recurrence of multiple PDACs through PanIN-like structures. Unique features and applications of this approach are discussed.

Materials and methods

Isolation of human pancreatic duct epithelial cells

Normal human pancreatic tissues were obtained with written consent from patients who underwent abdominal surgery for a pancreaticobiliary diseases. Human pancreatic duct epithelial cell (HPDEC4) was obtained from pancreas tail of a patient who underwent resection for pancreatic head carcinoma. No cancerous lesions near the specimen were confirmed by histopathological examination. HPDEC6 and HPDEC 7–11 were obtained from patients who underwent resection for solid pseudopapillary neoplasm and ampullary cancer, respectively. The pancreas tissue was confirmed macroscopically normal with no pathological lesions by pathologists, minced into pieces suspended in Hanks' balanced salt solution with 1 mg/ml Liberase HI (Roche) and incubated at 37°C for 60 min. The dissociated tissues were subsequently filtered with a 70 μm pores Cell Strainer (BD Biosciences) and isolated primary epithelial cells were seeded on type I collagen-coated dishes (Corning). HPDECs were maintained in serum-free keratinocyte serum-free medium (Invitrogen) supplemented with 5 ng/ml epidermal growth factor (Sigma), 50 μg/ml of bovine pituitary extract (Hammond CELL TECH), 10% fetal bovine serum, 2 mM NAC (N-Acetyl-L-cysteine; Wako), 0.2 mM Asc-2P (L-ascorbic acid 2-phosphate; Wako), which is similar to the K-NAC medium described earlier (9), but further supplemented with 5 μM Y-27632 (Selleck Chemicals).

Pancreatic cancer cell lines

Pancreatic cancer cell lines, AsPC-1, BxPC-3, Capan-1, Capan-2, HPAC, PANC-1 and MIAPaCa-1, were obtained from ATCC and grown in Dulbecco's modified Eagle's medium (DMEM; Nacalai tesque) containing 10% fetal bovine serum. These cell lines have not been authenticated by the authors.

Vector construction and retroviral infection

Oncogenic KRAS (KRAS^{G12V}) and a mutant form of MYC (MYC^{T58A}) generated by site-directed mutagenesis were cloned and recombined into retroviral expression vectors to generate pCLXSN-KRAS^{G12V}and pCMSCVpuro-MYC^{T58A}, as described previously (8). A retroviral vector pCLSI-MSCVhyg-H1R-p53shRNA was designed to express a p53-specific short

Abbreviations: DOX, doxycyclin; HPDEC, human pancreatic duct epithelial cell; HPV16, human papillomavirus 16; PanIN, Pancreatic Intraepithelial Neoplasia; shRNA, short hairpin RNA.

hairpin RNA (shRNA) targeting 5′-GACTCCAGTGGTAATCTAC-3′ (10). Lentiviral vectors expressing TERT, cyclin D1 and mutant CDK4 (CDK4^{R24C}; an inhibitor resistant form of CDK4) were constructed by recombination with a lentiviral vector, CSII-CMV-RfA as described previously (8). CSII-TRE-Tight-RfA was generated by replacing the elongation factor promoter in CSII-EF-RfA with the tetracycline-responsive promoter from pTRE-Tight (Clontech). CSII-TRE-Tight-16E6E7-2A-MYC^{T58A}-2A-HRAS^{G12V}(-KRAS^{G12V}) was constructed by inserting 16E6E7, MYC^{T58A} and HRAS^{G12V} (KRAS^{G12V}) segments separated by sequences encoding the autonomous 'self-cleaving' 2A peptides derived from foot-and-mouse disease virus into CSII-TRE-Tight-RfA. The production of recombinant viruses was as detailed earlier (8,11).

Ethics statement

Tissues from patients: Normal human pancreatic tissues were obtained with written consent from patients. The study was approved by the National Cancer Center Institutional Review Board. Animal study: Animal studies were carried out according to the Guideline for Animal Experiments in National Cancer Center, which meet the ethical standards required by the law and the guidelines about experimental animals in Japan, and approved by the Committee for Ethics in Animal Experimentation of the National Cancer Center. Cell line information: Pancreatic cancer cell lines, AsPC-1, BxPC-3, Capan-1, Capan-2, HPAC, PANC-1 and MIAPaCa-1, were directly obtained from ATCC. Among them AsPC-1, BxPC-3, PANC-1 and MIAPaCa-1 were purchased in 1993, and AsPC-1, BxPC-3, PANC-1 and MIAPaCa-1 were purchased in 2009. They have been passaged and used in our laboratory for <6 months after resuscitation though these cell lines have not been authenticated by the authors.

Western analysis

Western blotting was conducted as described previously (8). Antibodies used were listed in the Supplementary Materials and methods, available at *Carcinogenesis* Online.

G-banding karyotyping analysis

The karyotype analysis was carried out using standard G-banding by an outsourced service (Mitsubishi Chemical Medience).

Three-dimension culture for HPDECs

The three-dimensional culture protocol was a modification of the procedure described previously (12). Briefly, cells were embedded in type I collagen (final 2 mg/ml solution, AteloCell IPC; Koken) alone or in a mixture of type I collagen (final 2 mg/ml) and Matrigel (final 2 mg/ml, 354248; BD Biosciences) mixed with growth medium containing 10 mM HEPES. Cells were cultivated in the gel on a cell culture insert (353494, FALCON) dipped in growth medium for 3–4 weeks. For histological analysis, cultures were fixed with 10% neutral buffered Formalin (4% formaldehyde) and embedded in paraffin.

Immunohistochemical examination

Formalin-fixed and paraffin-embedded tissue sections were deparaffinized in xylene and rehydrated through a graded ethanol series (100–70%). For antigen retrieval, slides were immersed in a citrate buffer (pH 6.4) or Target Retrieval Solution (pH9) (S2367; Dako). The slides were then incubated in methanol containing 0.3% H_2O_2 to inhibit endogenous peroxidase activity. After washing, primary antibodies were applied for 1 h and binding was detected using an Envision Kit (Dako). Color development was achieved with 3, 3′-diaminobenzidine as chromogen and hematoxylin counterstaining.

Tumorigenesis in Nude Mice

All surgical procedures and care of the animals were in accordance with institutional guidelines. A 100 µl volume of 10^6 cells in a 1:1 mixture of Matrigel (354248; BD Biosciences) was subcutaneously injected into female BALB/c nude mice (Clea Japan). Doxycyclin (DOX) was given to the recipient mice via their drinking water (1 mg/ml in 5% sucrose). Tumor size was measured every other day using calipers and tumor volume was estimated using the following formula: $V = (LW^2)/2$, where V, volume (mm^3); L, largest diameter (mm) and W, smallest diameter (mm).

Results

Conditional tumorigenic transformation of primary HPDECs with human papillomavirus type 16 E6/E7, MYC and oncogenic RAS^{G12V}

Previously, we demonstrated that introduction of human papillomavirus type 16 (HPV 16) E6 and E7 genes (E6E7), oncogenic HRAS (HRAS^{G12V}) and MYC (MYC^{T58A}) is sufficient for tumorigenic transformation of normal human cells, such as cervical keratinocytes, tongue keratinocytes and bronchial epithelial cells (6–8). Here, a single polycistronic vector designed to express E6E7, MYC and KRAS^{G12V} (EMR) under control of a tetracycline-responsive promoter was transduced into a strain of primary HPDEC6 together with the tetracyclin-dependent transcriptional activator (tetOFF) (Figure 1A). DOX-dependent silencing of the oncogenes was confirmed by western blotting. The growth of HPDEC6 cells depended on expression of the transgenes (Figure 1B and C). When transduced cells were subcutaneously transplanted into nude mice, they formed tumors within 1 month (Table I, Figure 1D). Most parts of the resultant tumors showed histological features corresponding to moderately to poorly differentiated adenocarcinoma (Figure 1E, left panel) and some parts of periphery of the tumors showed those corresponding to well-differentiated adenocarcinoma (Figure 1E, middle panel). When the tumors became evident, DOX was administered to animals and this resulted in halted tumor growth, followed by almost complete regression. Close examination of the remaining tissues showed ductal structures consisting of simple columnar epithelium (Figure 1E, right panel). The epithelial cells derived from HPDEC maintained quasinormal duct structures for at least 1 month in subcutaneous sites of mice without any sign of tumor growth.

After confirmation of regression of initial tumors, DOX was withdrawn to examine whether tumors regrew or not. About 2 months after the withdrawal, overt tumors reappeared at the sites of initial tumors. Interestingly, a mixed histology composed of simple columnar cells and malignant cells was observed in the reformed tumors (Supplementary Figure 1C, available at *Carcinogenesis* Online).

In a genetic engineered tumor model of *Rattus* pancreas, expression of oncogenic *Kras* or *Hras* induces pancreatic cancer, whereas in human lesions, oncogenic KRAS mutations are most common (13). In our xenograft model, HRAS^{G12V} showed essentially the same results as obtained with KRAS^{G12V} (Figure 1D and E; Supplementary Figure 1A, available at *Carcinogenesis* Online). We confirmed the tumorigenic effects of the oncogenes by employing another independent batch of HPDEC derived from other patients (Supplementary Figure 1B, available at *Carcinogenesis* Online). These results support that oncogenic RAS signaling plays a crucial role in pancreatic cancer development.

Temporal analyses of PDAC development from quasinormal tissues derived from HPDEC

To more precisely characterize the histological features of the tumors and to analyze the temporal development of tumors from quasinormal ductal structures, tumors were collected and examined at different time points before and after DOX administration, and after withdrawal of DOX.

As in the pilot experiment described above, initial tumors appeared within 1 month, and the tumor volume exceeded 300 mm^3 within 20 days, when DOX was administered. After the initial tumors regressed to masses <150 mm^3, DOX was withdrawn. Reproducibility of not only the initial tumor growth but also the regression and regrowth of the tumors was excellent, judging from the standard error bars of the tumor sizes of individual animals and even tumor sizes for different animals (Figure 2A). The initial tumors were confirmed to exhibit moderately to poorly differentiated adenocarcinoma histology (Figure 2B). Immunohistochemical analyses indicated that the tumors expressed MUC1 and MUC5AC, which are also widely expressed in human PDAC clinical samples. On the other hand, expression of CDX-2 and MUC6 was not detected (Figure 2C). Thus, the initial tumors derived from HPDEC6-*tre* EMR cells resemble human PDACs in terms of microscopic histology and immunohistochemical expression pattern.

Subsequently, we examined regulation of transgenes *in vivo* by immunohistochemical detection of MYC protein. The initial tumors which should express EMR showed strong staining of MYC, whereas no expression was detected in the epithelial cells in the tissues remaining after DOX administration for 60 days. Staining for Ki67 indicated that repression of the oncogenes reduced cell proliferation (Figure 2B). These results confirmed that regulation of oncogene expression also functioned *in vivo* as well as *in vitro*.

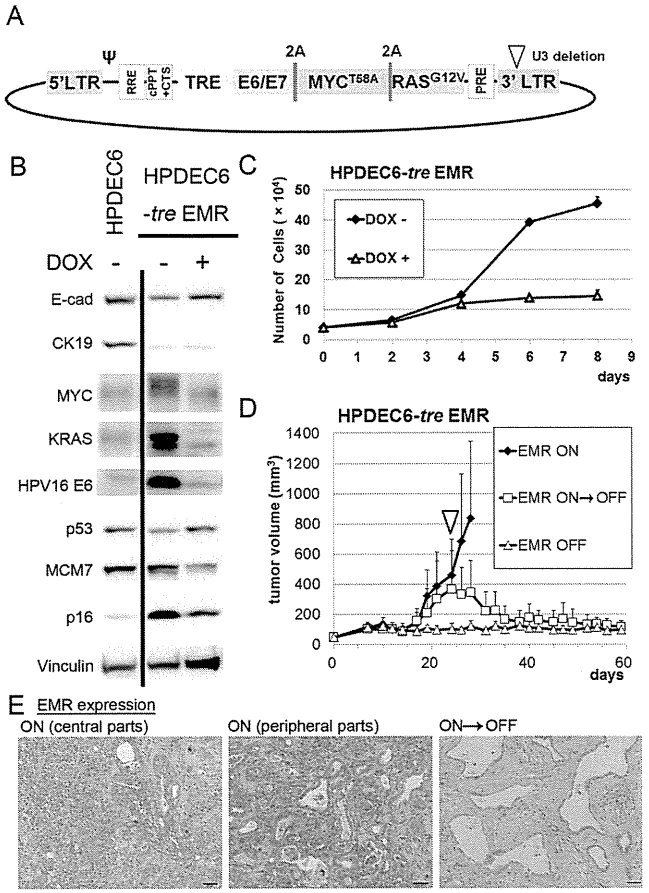

Fig. 1. Expression of HPV16 E6E7, KRAS^{G12V} and MYC^{T58A} is sufficient for full transformation of primary human pancreatic duct cells. (**A**) Schematic illustration of a single polycistronic lentiviral vector in which expression of E6E7, MYC^{T58A} and KRAS^{G12V} (EMR) is regulated by DOX (tetOFF). TRE, tetracyclin-responsive elements; 2A, 'self-cleaving' 2A peptides derived from foot-and-mouse disease virus, ψ, packaging signal regions; RRE, rev responsive element; cPPT, central polypurine tract; CTS, central termination sequence; PRE, woodchuck hepatitis virus posttranscriptional regulatory element. (**B**) Expression of the transgene products and several target proteins possibly regulated by them was determined by western blotting. Lane 1, parental HPDEC6 cells at passage 8. Lanes 2 and 3, HPDEC6 cells transduced with EMR and tetOFF at passage 9 were propagated and treated with 1 μg/ml DOX (DOX+) or vehicle (DOX–) for 5 days at passage 16. (**C**) Growth curves of HPDEC6-*tre* EMR cells with or without DOX. Cells were seeded at a density of 4×10^4 cells per 22 mm dish (BD Biosciences) at day 0 and counted at the indicated days. DOX (1 μg/ml) or vehicle (70% ethanol) was added from day 2 and thereafter every other day with fresh medium. Each point is the mean of the triplicates ± standard deviation. (**D**) Tumor-forming ability of HPDEC6-*tre* EMR. Cells were subcutaneously injected into nude mice (1×10^6 cells) and tumor size was measured every other day. One mouse was fed with drinking water supplemented with 1 mg/ml DOX from day 0 (open triangles). Of the other two mice, one mouse was administered with DOX from day 24 (white arrowhead) when the mean tumor volume exceeded 300 mm^3 (open rectangles). Each point is the mean of the tumor volume ± standard deviation ($n = 6$). (**E**) Histopathology of the xenografts stained with hematoxylin and eosin. A representative image of central parts of the tumors, which corresponds to moderately to poorly differentiated carcinoma (left panel), and that of peripheral parts of the tumors, which corresponds to well-differentiated adenocarcinoma from the mouse without DOX administration (closed rhombuses in D) killed at day 28. Right panel shows a representative image of the remaining tissue from the mouse after tumor regression by DOX administration (open squares in D) killed at day 60. Scale bars, 50 μm.

MYC reexpression was detected at as early as 6 days after DOX withdrawal and significant increase of Ki-67 positive cells was detected at day 12, when overt tumor growth was observed. Mixed histology composed of simple columnar epithelium, well-differentiated adenocarcinomas and undifferentiated carcinomas was observed at day 21. The population of undifferentiated cells showed strong staining of MYC and Ki67 was present, whereas staining of CK19 and MUC1 was very weak (Figure 2D). In contrast, the cells of simple epithelium were negative for MYC and Ki67 and positive for CK19 and/or MUC1. Intriguingly, the cells used for transplantation were near diploid, and 45% (9/20) were normal diploid (Supplementary Table 1, available at *Carcinogenesis* Online), although it has been reported that HPV16 E6 and E7 readily induce chromosomal instability and tetraploidy (14–16). Taken together, these results suggest that E6E7, oncogenic RAS and MYC are sufficient for tumorigenic transformation of primary HPDECs without further genetic alterations.

Immortalization of normal HPDECs

We could conditionally immortalize and transform primary HPDECs with the four oncogenes and observe transition of quasinormal HPDEC-derived duct-like structures to PanIN-like and PDAC-like histological structures in mouse xenografts. However, this model does not faithfully mimic pancreatic carcinogenesis since four oncogenes were expressed at the same time and HPV is not considered to be at all involved in human PDAC development. To analyze events of PDAC development, normal HPDECs should be freely cultivated *in vitro*. However, no normal HPDEC lines have been available except for a HPDEC line immortalized with HPV16 E6 and E7, and reliable methods for long-term culture of HPDECs have been lacking (9). As we recently found that a ROCK inhibitor, Y27632, could inhibit keratinocyte differentiation through a novel NOTCH-ROCK pathway (17), we applied it to the reported medium for HPDEC culture. With the modified method, plating efficiencies of HPDECs were remarkably improved, but they eventually stopped growing after 9–38 population doublings depending on cell batches (Figure 3A and B). As senescence of normal human epithelial cells in regular culture conditions is caused by activation of RB and telomere shorting, we tried to immortalize the cells by activating telomerase through transduction of TERT, and by inactivating the pRB pathway with mutant CDK4 (CDK4^{R24C}, an inhibitor resistant form of CDK4) and cyclin D1, into primary HPDECs with lentiviral vectors (18). With this strategy, we could immortalize pooled populations of HPDEC-4, -6, -8 and -10. The combination of CDK4^{R24C}, cyclin D1 and TERT (K4DT) clearly extended the life span over 40 population doublings and virtually immortalized HPDEC10 cells, whereas TERT alone hardly extend the life span (Figure 3A). Expression of the transgenes was confirmed by immunoblotting (Figure 3B). The immortalized HPDECs, as well as the primary cells, expressed cytokeratin 19 and E-cadherin (Figure 3C). Among them karyotype of HPDEC4-K4DT, HPDEC8-K4DT and HPDEC10-K4DT cells were analyzed and revealed that the majority of the cells were normal diploid (Supplementary Table 1, available at *Carcinogenesis* Online), indicating this is an efficient strategy to immortalize normal HPDECs with minimal alteration of the genetic background.

In three-dimensional culture with type I collagen as the extracellular matrix, HPDEC4-K4DT cells could form duct-like structures in the gel (Figure 3D), suggesting retention of a biological characteristic of HPDECs after immortalization. This could be a good tool to examine early carcinogenic events.

Tumorigenic transformation of HPDEC4-K4DT cells with transduction of p53-specific shRNA, KRAS^{G12V} and MYC

Since HPDEC4-K4DT cells were pooled populations established from primary culture of pancreatic tissue, proliferation of mesenchymal cells sometimes compromised that of epithelial cells, although the majority of HPDEC4-K4DT cells appeared to be epithelial in nature. To remove mesenchymal cells, we cloned epithelial cell lines by limiting dilution. Then, we examined the effects of several oncogenes relevant to pancreatic carcinogenesis on the HPDEC4-B7 cell line, a purified epithelial cell line with normal diploidy. Since, the pRB pathway was already inactivated and telomerase activated in the cells, we tested three genetic alterations; inactivation of p53 using shRNA,

Table I. Summary of xenotransplantation of HPDECs

Cells	Number of tumors per subcutaneous injection
HPDEC6	
-*tre* E6E7-MYC^{T58A}-KRAS^{G12V}	6/6 (28) [exp 1; Figure 1] [a]5/6 (26) [exp 2; Figure 2]
-*tre* E6E7-MYC^{T58A}-HRAS^{G12V}	6/6 (28) [Supplementary Figure 1, available at *Carcinogenesis* Online)]
HPDEC4	
-*tre* E6E7-MYC^{T58A}-HRAS^{G12V}	6/6 (3) [Supplementary Figure 1, available at *Carcinogenesis* Online] 4/6 (59) [Supplementary Figure 1, available at *Carcinogenesis* Online; reexpression)]
HPDEC4-K4DT (B7)	
-p53 shRNA-KRAS^{G12V}-MYC^{T58A}	6/6 (48) [Figure 4]
-p53 shRNA-KRAS^{G12V}-vector	4/6 (98) [Figure 4]
-p53 shRNA- MYC$^{T58A\text{-vector}}$	0/6 (100)
-Luc shRNA-KRAS^{G12V}-MYC^{T58A}	0/6 (100)
-p53 shRNA-vector-vector	0/6 (100)

Numbers in parentheses indicate observation time points (days) when mice were killed.
[a]Note that one of the six tumors was less than the criterial volume (150 mm^3), but it exhibited adenocarinoma-like histology. Words in square brackets are information of experiment number and related figure.

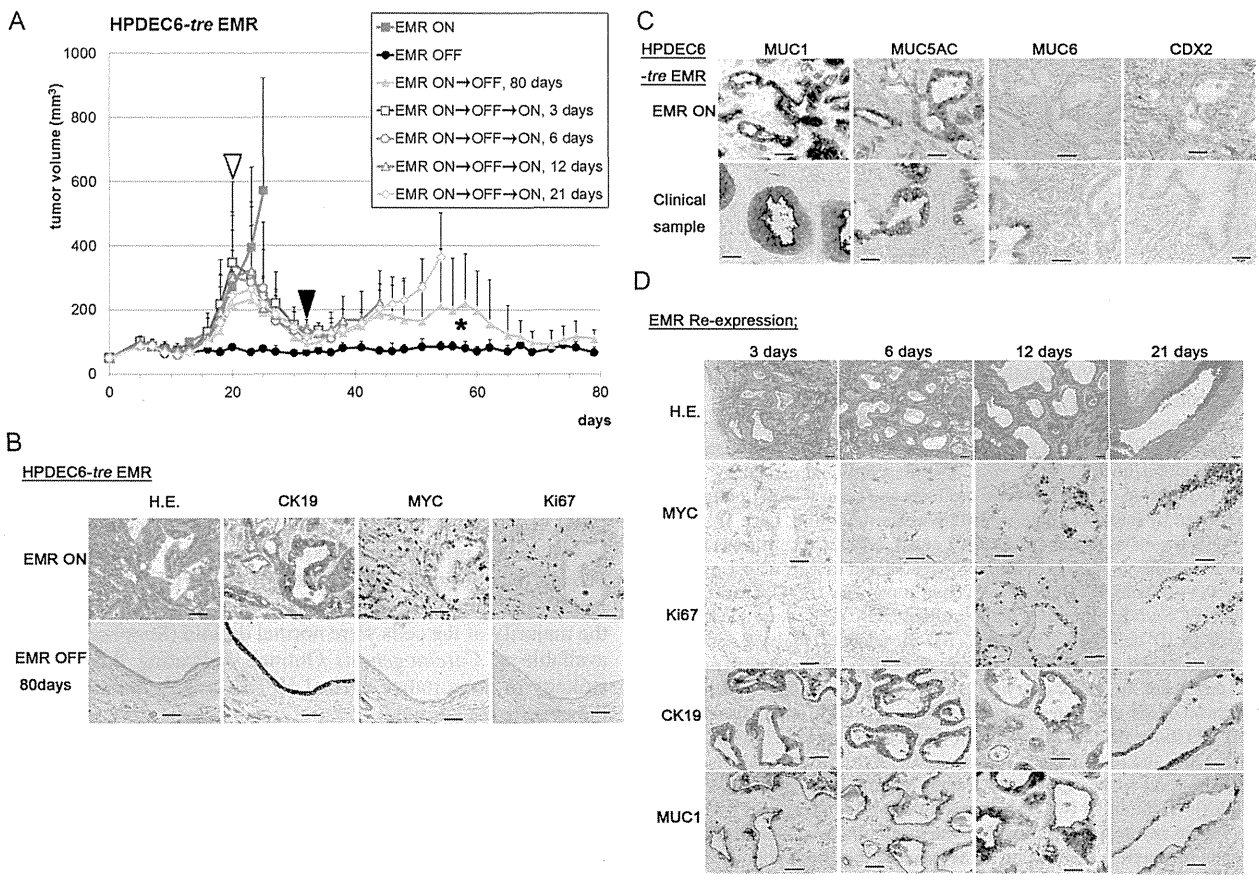

Fig. 2. Development of PDAC-like tumors from quasinormal tissues derived from HPDEC6-*tre* EMR cells. (**A**) Growth curves of the tumors. HPDEC6-*tre* EMR cells were subcutaneously injected into nude mice (1×10^6 cells). One mouse was administered with DOX from day 0 as described in Figure 1D (black closed circles). Among the other six mice, one mouse was killed at day 26 as mean tumor volume exceeded 500 mm^3 (red closed squares) and five mice were administered with DOX from day 20 (white arrowhead) until day 31 when all the tumors regressed almost completely. Then DOX administration to four mice was discontinued at day 32 (black arrowhead), and the mice were killed at different time points as indicated, namely 3 days (purple open squares), 6 days (orange open circles), 12 days (blue open triangles) and 21 days (green open rhombuses) after the DOX withdrawal. The other mouse was continuously administered with DOX until day 80 (green closed triangles). *Note that the apparent increase of the tumor volume around day 40–60 in this mouse was due to cyst-like soft mass formation but not solid tumors. Each point is the mean of the tumor volume ± standard deviation ($n = 6$). (**B**) Histopathology of subcutaneous tumors of the mouse killed at day 26 and remaining tissues after tumor regression in the mouse killed at day 80. (**C**) Immunohistochemical comparison of the PDAC-like tumors and a typical human PDAC. Expression of MUC1, MUC5AC, MUC6 and CDX2 were examined. Note that positive signals in the xenograft by CDX2 staining were localized at the positions where Matrigel remained. (**D**) Development of PDAC-like tumors from the quasinormal pancreatic duct-like structures subcutaneously formed in mice. Temporal development of tumors were analyzed by hematoxylin and eosin staining and immunohistochemical staining of MYC, Ki67, CK19 and MUC1. Scale bars represent 50 μm.

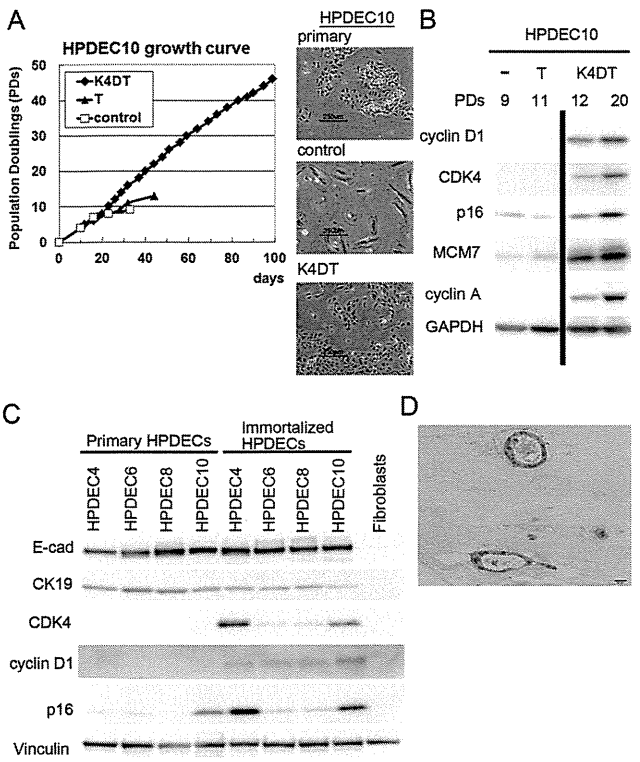

Fig. 3. Immortalization of primary HPDECs. (**A**) Growth curves of HPDEC10 cells transduced by indicated genes at passage 0. The cells transduced with mutant CDK4, cyclin D1 and TERT (K4DT) were virtually immortalized and maintained epithelial cell morphology without growth retardation, whereas TERT-transduced cells (T) and control cells senesced around population doublings 10. Scale bars, 250 μm. (**B**) Expression of CDK4 and cyclin D1 as well as some cell cycle-associated genes were examined by western blotting. (**C**) Expression of the transgenes and duct epithelial markers in four batches of primary HPDECs and those immortalized by transduction of K4DT were confirmed by western blotting. Fibroblasts derived from the same pancreatic tissue from which HPDEC4 cells were obtained were used as a control. (**D**) HPDEC4-K4DT cells were cultivated in a collagen gel for 4 weeks and fixed, paraffin embedded, sectioned and stained with hematoxylin and eosin. A scale bar represents 20 μm.

introduction of oncogenic KRAS and altered expression of MYC. Combinations of p53-specific shRNA (p53shRNA), $KRAS^{G12V}$ and MYC were serially transduced into HPDEC4-B7 cells. Expression of KRAS, MYC and downregulation of p53 were confirmed by western blotting. The expression levels of transgenes were comparable with those of pancreatic cancer cell lines (Figure 4A).

In three-dimensional culture, p53 shRNA-expressing HPDEC4-B7 cells formed larger duct-like structures than control shRNA-expressing cells, which formed similar duct-like structures as the parental pooled HPDEC4-K4DT cells (Figure 4B). In accordance with the larger duct-like structures formed by HPDEC4-B7-p53shRNA cells, most showed Ki67 staining. To examine effects of $KRAS^{G12V}$ expression, we compared HPDEC4-B7-p53shRNA and HPDEC4-B7-p53shRNA-$KRAS^{G12V}$ cells, since oncogenic RAS might further induce p53 expression (19). With $KRAS^{G12V}$ expression, PanIN-like structures were recapitulated and most of p53shRNA-$KRAS^{G12V}$ cells were positive for Ki-67 staining (Figure 4B and C). In this system, the cells already express $KRAS^{G12V}$ before being embedded in the gel, which is not the real situation for early events in carcinogenesis. So we also tried conditional $KRAS^{G12V}$ expression by DOX in 3D culture, but failed to observe formation of PanIN-like structures, although induction of $KRAS^{G12V}$ did support faster proliferation of cells in monolayer culture (Supplementary Figure 2, available at *Carcinogenesis* Online).

To examine tumorigenic ability, 1×10^6 cells were injected subcutaneously into nude mice. HPDEC4-B7-p53shRNA-$KRAS^{G12V}$-MYC^{T58A}-expressing cells formed tumors within 2 months, whereas p53shRNA- and $KRAS^{G12V}$-expressing cells formed tumors only after a long latent period (Figure 4D). Tumors derived from HPDEC4-B7 cells histologically were poorly differentiated adenocarcinomas and expressed MUC1/MUC5AC as HPDEC6-*tre* EMR cells did (Figure 4E). The other combinations of the transgenes did not confer tumorigenicity on the cells (Figure 4D, Table I).

Notably, 40% (8/20) of HPDEC4-B7-p53shRNA-$KRAS^{G12V}$-MYC^{T58A} cells were normal diploid (Supplementary Table 1, available at *Carcinogenesis* Online). These results again indicate that KRAS and MYC on a background of inactivation of pRB and p53 pathways and active telomerase are sufficient for tumorigenic transformation of normal HPDECs without further genetic alterations.

Discussion

Establishment and *in vitro* culture of normal human pancreatic cells is important not only for determination of genetic alterations required for malignant transformation but also as ideal controls for identifying therapeutic targets specific for cancer cells. However, *in vitro* cultures of normal human pancreatic cells are very limited. Thus, most *in vitro* models for human PDACs have utilized established cancer cell lines. Nevertheless, there are a few human pancreatic epithelial cell lines immortalized with HPV16 E6 and E7 or ectopic expression of TERT (9,20). It has been shown that HPV16 E6 and E7, oncogenic $Kras^{G12D}$ and SV40 small t antigen are sufficient to transform TERT-immortalized HPDECs, and oncogenic KRAS alone can transform human pancreatic epithelial cells preimmortalized with HPV16 E6 and E7 (20,21). In the present report, we document that HPV16 E6 and E7, oncogenic RAS and MYC are sufficient to transform primary normal HPDECs. Furthermore, oncogenic RAS and inactivation of p53 are sufficient to transform HPDECs immortalized with $CDK4^{R24C}$, cyclin D1 and TERT. All these results suggest that the number of genetic alterations required for malignant transformation is much smaller than the average of 48 alterations detected by global direct sequencing (22,23).

Numerous genetically engineered mouse models mimicking PanINs, intraductal papillary mucinous neoplasm, mucinous cystic neoplasms and PDACs have been successfully developed in recent years (5,24–27). However, *in vitro* cultures of the human counterparts are not available. No study has succeeded in recapitulating precancerous lesions *ex vivo*. Better understanding of the genetics of precancerous lesions is essential for their early detection and prophylaxis. In this study, we succeeded in reconstructing ductal structures consisting of simple columnar epithelium with primary HPDECs, conditionally expressing four oncogenes sufficient for malignant transformation. From the quasinormal duct structures, development of PDACs through PanIN-like structures could be observed. Our methodology described in here could be applied to many other cell types, since we have demonstrated that HPV16 E6 and E7, oncogenic RAS and MYC are sufficient to transform different types of normal human cells (6,8,28).

Four genes, KRAS, p16/CDKN2A, p53 and DPC4/SMAD4 are most commonly mutated or inactivated in PDACs. These are classified as driver alterations for PDAC development. In the majority of not only PDACs but also many other cancers, telomerase is activated and overexpression of MYC is observed. The tumors in this report presented some typical features of PDAC, even when etiologically irrelevant HPV16 oncogenes were used for transformation (29). This might not be surprising since the viral oncogenes can mimic frequent alterations found in PDACs, namely E6 targets p53 for degradation and activates telomerase and E7 binds and inactivates pRB. Our tumorigenic cells harbored normal diploid or near diploid chromosomes, suggesting combinations of these transgenes are sufficient for malignant transformation without further genetic alteration. The experimental results allow us to conclude that the mechanisms of how the two major tumor suppressor pathways are inactivated and the

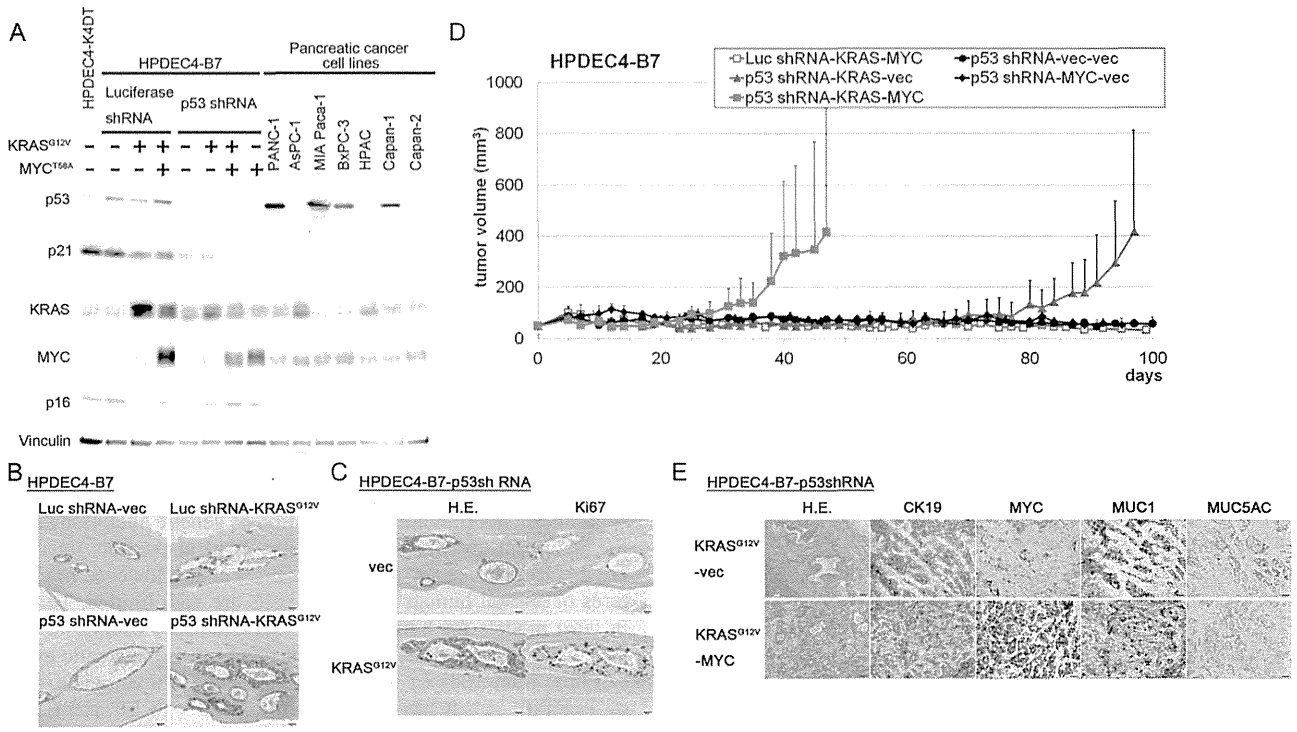

Fig. 4. Transduction of p53 shRNA, KRAS^{G12V} and MYC^{T58A} confers tumorigenicity to immortalized HPDECs in nude mice. (**A**) Clonal HPDEC4-B7 cells established from HPDEC4-K4DT cells were serially infected with p53 shRNA-, KRAS^{G12V}- and MYC^{T58A}-expressing retroviruses. Expression of KRAS, MYC, p53 as well as p21 and p16 was examined in comparison with those in several pancreatic cancer cell lines by western blotting. (**B** and **C**) HPDEC4-B7 cell lines expressing indicated transgenes were cultivated in a mixture of collagen type I and Matrigel. Formation of duct-like structures were analyzed as described in Figure 3D. (**B**) HPDEC4-B7-Luc shRNA-vec cells reconstituted duct-like structures in 3 weeks (upper left panel). The addition of p53 shRNA contributed to formation of large duct structures (lower left panel). Expression of KRAS^{G12V} and p53 shRNA induced dysplastic epithelial structures similar to PanIN, whereas KRAS^{G12V} expression alone did not (right panels). Scale bars represent 20 μm. (**C**) The PanIN-like structures formed by HPDEC4-B7-p53shRNA-KRAS^{G12V} cells were stained for Ki67. Hematoxylin and eosin (H.E.) staining (left panels) and Ki67 staining (right panels) are shown. Note that most of the cells were positive for Ki-67 staining, whereas the cells expressing p53-shRNA alone were not. Scale bars represent 20 μm. (D) Tumor growth curves of the HPDEC4-B7 cell lines with indicated transgenes. Cells were subcutaneously injected into nude mice (10^6 cells). The mouse transplanted with HPDEC4-B7-p53shRNA-KRAS^{G12V}-MYC^{T58A} was killed at 47 days (red squares) when tumors arose from all the six injected sites, whereas that with HPDEC4-B7-p53shRNA and KRAS^{G12V} was killed at 97 days (purple triangles) when large tumors grew from four out of six injected sites. The other cells did not show tumorigenicity within 3 months. Each point is the mean of the tumor volume ± standard deviation (n = 6). (**E**) Histological and immunohistochemical examination of the resultant tumors. Note that the xenograft tumors exhibited histological and immunohistochemical features similar to those of PDACs. Scale bars represent 50 μm.

telomerase is activated, do not greatly affect the resultant phenotypes of the tumors.

On the other hand, transduction of p53shRNA and KRAS^{G12V} in HPDECs immortalized with CDK4^{R24C}, cyclin D1 and TERT also formed tumors but only after a long latent period. Thus, it is clear that MYC expression facilitated tumor formation. This result is consistent with a previous report that HPV16 E6/E7 and oncogenic KRAS-expressing pancreatic cells showed inconsistent and rather weak tumorigenic potential (21). In the literature, resultant tumorigenic cells have been reported to show activation of AKT and the nuclear factor-κB pathway, which are also observed in PDACs (30,31). Overexpression of NFAT, activation of NOTCH signaling and Wnt/beta-catenin signaling are further features of PDACs (32–34). The available findings point to MYC as a possible convergent downstream target of these different pathways. Indeed, numerous studies have revealed that MYC gene amplification and overexpression contribute to malignant phenotype, and to progression of tumors (35,36).

We closely examined the remaining tissue after tumor regression by DOX administration in order to confirm that no tumor cells remained. Surprisingly, many ductal structures consisting of simple columnar epithelium were apparent. During regression, most tumor cells exhibited features of apoptotic cell death upon DOX administration (Supplementary Figure 3, available at *Carcinogenesis* Online). However, some survived to reform quasinormal ductal structures. Such cells were histologically attached to the basement membrane-like structures. Therefore, it is possible that only cells in a niche which can support survival of normal cells remained. These results might have important implications. Once driver oncogenes could be completely shut-off with specific inhibitors, tumor cells could reverse to normal. Reconstitution of normal tissue architectures of human cells *ex vivo* could be generally obtained by transplantation of the cells in the renal capsule of immunodeficient mice. However, our model system with reversible control of oncogene expression, to our knowledge for the first time, enabled quasinormal human pancreatic duct tissues to be formed subcutaneously in mice.

In recent years, development of drugs targeting RAS and MYC has been reported (37–39). However, normal cells could relapse when administration of the drugs was terminated. This seems to be the situation with many kinase inhibitors, even in the greatest success case of chronic myeloid leukemia treated with imatinib mesylate (Gleevec). To overcome such relapse, considerations of oncogene addiction and synthetic lethality have been emphasized to develop new therapeutic drugs (40). Indeed, the use of experimentally immortalized and transformed mammary epithelial cells has succeeded in identifying selective inhibitors of cancer stem cells using high-throughput screening (41). Since our methodology allows propagation of both normal and cancer-initiating cells under the same conditions *in vitro*, it should provide an ideal set of cells for screening of drugs for this purpose. Also it enabled *de novo* development of PDAC from preformed quasinormal human tissues and might be applicable to carcinogenesis models of any cancers.

Supplementary material

Supplementary Table 1 and Figures 1–5 can be found at http://carcin.oxfordjournals.org/

Funding

National Cancer Center Research and Development Fund (23-B-1 to T.K., 23-A-38 to T.K.); Grant-in-Aid for Cancer Research from the Ministry of Health Labor and Welfare of Japan (10103828 to T.K.); Princess Takamatsu Cancer Research Fund (10-24206 to T.K.); Scientific Research from the Ministry of Education, Culture, Sports, Science, and Technology of Japan (23300345 to T.K.).

Acknowledgements

The authors thank the members of the Department of Hepatobiliary and Pancreatic Surgery for clinical samples, Dr H.Miyoshi (RIKEN, BioResource Center) for lentiviral constructs and Dr M.Fujita (Kyushu University) for anti-MCM7 antibody. We would like to express our appreciation to T.Ishiyama, A.Noguchi and National Cancer Center Research Core Facility for their expert technical assistance.

Conflict of Interest Statement: None declared.

References

1. Vincent,A. *et al.* (2011) Pancreatic cancer. *Lancet*, **378**, 607–620.
2. Morris,J.P. 4th *et al.* (2010) KRAS, Hedgehog, Wnt and the twisted developmental biology of pancreatic ductal adenocarcinoma. *Nat. Rev. Cancer*, **10**, 683–695.
3. Mihaljevic,A.L. *et al.* (2010) Molecular mechanism of pancreatic cancer–understanding proliferation, invasion, and metastasis. *Langenbecks. Arch. Surg.*, **395**, 295–308.
4. Siegel,R. *et al.* (2014) Cancer statistics, 2014. *Cancer J. Clin.*, **64**, 9–29.
5. Pérez-Mancera,P.A. *et al.* (2012) What we have learned about pancreatic cancer from mouse models. *Gastroenterology*, **142**, 1079–1092.
6. Zushi,Y. *et al.* (2011) An in vitro multistep carcinogenesis model for both HPV-positive and -negative human oral squamous cell carcinomas. *Am. J. Cancer Res.*, **1**, 869–881.
7. Sasaki,R. *et al.* (2009) Oncogenic transformation of human ovarian surface epithelial cells with defined cellular oncogenes. *Carcinogenesis*, **30**, 423–431.
8. Narisawa-Saito,M. *et al.* (2012) A critical role of MYC for transformation of human cells by HPV16 E6E7 and oncogenic HRAS. *Carcinogenesis*, **33**, 910–917.
9. Furukawa,T. *et al.* (1996) Long-term culture and immortalization of epithelial cells from normal adult human pancreatic ducts transfected by the E6E7 gene of human papilloma virus 16. *Am. J. Pathol.*, **148**, 1763–1770.
10. Nair,A.R. *et al.* (2005) Inhibition of p53 by lentiviral mediated sh RNA abrogates G1 arrest and apoptosis in retinal pigmented epithelial cell Line. *Cell Cycle*, **4**, 697–703.
11. Carey,B.W. *et al.* (2009) Reprogramming of murine and human somatic cells using a single polycistronic vector. *Proc. Natl Acad. Sci. USA.*, **106**, 157–162.
12. Ootani,A.*et al.* (2009) Sustained in vitro intestinal epithelial culture within a Wnt-dependent stem cell niche. *Nature Medicine*, **15**, 1–U140.
13. Tanaka,H. *et al.* (2010) Mature acinar cells are refractory to carcinoma development by targeted activation of Ras oncogene in adult rats. *Cancer Sci.*, **101**, 341–346.
14. Duensing,S. *et al.* (2002) The human papillomavirus type 16 E6 and E7 oncoproteins independently induce numerical and structural chromosome instability. *Cancer Res.*, **62**, 7075–7082.
15. Duensing,S. *et al.* (2000) The human papillomavirus type 16 E6 and E7 oncoproteins cooperate to induce mitotic defects and genomic instability by uncoupling centrosome duplication from the cell division cycle. *Proc. Natl Acad. Sci. USA*, **97**, 10002–10007.
16. Hashida,T. *et al.* (1991) Induction of chromosome abnormalities in mouse and human epidermal keratinocytes by the human papillomavirus type 16 E7 oncogene. *J. Gen. Virol.*, **72**(Pt 7), 1569–1577.
17. Yugawa,T. *et al.* (2013) Noncanonical NOTCH signaling limits self-renewal of human epithelial and induced pluripotent stem cells through ROCK activation. *Mol. Cell. Biol.*, **33**, 4434–4447.
18. Kiyono,T. (2007) Molecular mechanisms of cellular senescence and immortalization of human cells. *Expert Opin. Ther. Targets*, **11**, 1623–1637.
19. Serrano,M. *et al.* (1997) Oncogenic ras provokes premature cell senescence associated with accumulation of p53 and p16INK4a. *Cell*, **88**, 593–602.
20. Campbell,P.M. *et al.* (2007) K-Ras promotes growth transformation and invasion of immortalized human pancreatic cells by Raf and phosphatidylinositol 3-kinase signaling. *Cancer Res.*, **67**, 2098–2106.
21. Qian,J. *et al.* (2005) *In vitro* modeling of human pancreatic duct epithelial cell transformation defines gene expression changes induced by K-ras oncogenic activation in pancreatic carcinogenesis. *Cancer Res.*, **65**, 5045–5053.
22. Feldmann,G. *et al.* (2009) *In vitro* models of pancreatic cancer for translational oncology research. *Expert Opin. Drug Discov.*, **4**, 429–443.
23. Jones,S. *et al.* (2008) Core signaling pathways in human pancreatic cancers revealed by global genomic analyses. *Science*, **321**, 1801–1806.
24. Hingorani,S.R. *et al.* (2003) Preinvasive and invasive ductal pancreatic cancer and its early detection in the mouse. *Cancer Cell*, **4**, 437–450.
25. Siveke,J.T. *et al.* (2007) Concomitant pancreatic activation of Kras(G12D) and Tgfa results in cystic papillary neoplasms reminiscent of human IPMN. *Cancer Cell*, **12**, 266–279.
26. Mao,J. *et al.* (2006) A novel somatic mouse model to survey tumorigenic potential applied to the Hedgehog pathway. *Cancer Res.*, **66**, 10171–10178.
27. Izeradjene,K. *et al.* (2007) Kras(G12D) and Smad4/Dpc4 haploinsufficiency cooperate to induce mucinous cystic neoplasms and invasive adenocarcinoma of the pancreas. *Cancer Cell*, **11**, 229–243.
28. Narisawa-Saito,M. *et al.* (2008) An *in vitro* multistep carcinogenesis model for human cervical cancer. *Cancer Res.*, **68**, 5699–5705.
29. Nagata,K. *et al.* (2007) Mucin expression profile in pancreatic cancer and the precursor lesions. *J. Hepatobiliary. Pancreat. Surg.*, **14**, 243–254.
30. Navas,C. *et al.* (2012) EGF receptor signaling is essential for k-ras oncogene-driven pancreatic ductal adenocarcinoma. *Cancer Cell*, **22**, 318–330.
31. Ling,J. *et al.* (2012) KrasG12D-induced IKK2/β/NF-κB activation by IL-1α and p62 feedforward loops is required for development of pancreatic ductal adenocarcinoma. *Cancer Cell*, **21**, 105–120.
32. Köenig,A. *et al.* (2010) NFAT-induced histone acetylation relay switch promotes c-Myc-dependent growth in pancreatic cancer cells. *Gastroenterology*, **138**, 1189–99.e1.
33. Mazur,P.K. *et al.* (2010) Notch2 is required for progression of pancreatic intraepithelial neoplasia and development of pancreatic ductal adenocarcinoma. *Proc. Natl Acad. Sci. USA*, **107**, 13438–13443.
34. Zhang,Y. *et al.* (2013) Canonical wnt signaling is required for pancreatic carcinogenesis. *Cancer Res.*, **73**, 4909–4922.
35. Wolfer,A. *et al.* (2010) MYC regulation of a "poor-prognosis" metastatic cancer cell state. *Proc. Natl Acad. Sci. USA*, **107**, 3698–3703.
36. Schleger,C. *et al.* (2002) c-MYC activation in primary and metastatic ductal adenocarcinoma of the pancreas: incidence, mechanisms, and clinical significance. *Mod. Pathol.*, **15**, 462–469.
37. Shima,F. *et al.* (2013) In silico discovery of small-molecule Ras inhibitors that display antitumor activity by blocking the Ras-effector interaction. *Proc. Natl Acad. Sci. USA*, **110**, 8182–8187.
38. Zimmermann,G. *et al.* (2013) Small molecule inhibition of the KRAS-PDEδ interaction impairs oncogenic KRAS signalling. *Nature*, **497**, 638–642.
39. Zirath,H. *et al.* (2013) MYC inhibition induces metabolic changes leading to accumulation of lipid droplets in tumor cells. *Proc. Natl Acad. Sci. USA.*, **110**, 10258–10263.
40. Kaelin,W.G. Jr. (2005) The concept of synthetic lethality in the context of anticancer therapy. *Nat. Rev. Cancer*, **5**, 689–698.
41. Gupta,P.B. *et al.* (2009) Identification of selective inhibitors of cancer stem cells by high-throughput screening. *Cell*, **138**, 645–659.

Received January 23, 2014; revised April 9, 2014; accepted May 3, 2014

doi 10.1700/1636.17918

Tumori 2014;100(4):e99-e106

Potential diagnostic biomarkers: differential expression of LMP2/β1i and cyclin B1 in human uterine leiomyosarcoma

Takuma Hayashi[1,10,11], Akiko Horiuchi[2], Kenji Sano[3], Nobuyoshi Hiraoka[4], Tomoyuki Ichimura[5], Tamotsu Sudo[6], Osamu Ishiko[5], Nobuo Yaegashi[7], Hiroyuki Aburatani[8], and Ikuo Konishi[9]

[1]Department of Immunology and Infectious Disease, Shinshu University Graduate School of Medicine, Matsumoto; [2]Horiuchi Ladies Clinic, Matsumoto; [3]Department of Laboratory Medicine, Shinshu University Hospital, Matsumoto; [4]Pathology Division, National Cancer Center Research Institute, Tokyo; [5]Department of Obstetrics and Gynecology, Osaka City University Graduate School of Medicine, Osaka; [6]Department of Gynecology, Hyogo Cancer Center, Hyogo; [7]Department of Obstetrics and Gynecology, Tohoku University Graduate School of Medicine, Sendai; [8]The Cancer System Laboratory, Research Center for Advanced Science and Technology, The University of Tokyo, Tokyo; [9]Department of Obstetrics and Gynecology, Kyoto University Graduate School of Medicine, Kyoto;[10]Promoting Business Using Advanced Technology, Japan Science and Technology Agency (JST), Tokyo, Japan; [11]SIGMA-Aldrich Collaboration Laboratory, Rehovot, Israel

Key words: LMP2, cyclin B1, uterine leiomyosarcoma, diagnostic biomarker.

Acknowledgments: We sincerely thank Professors Susumu Tonegawa (Massachusetts Institute of Technology) and Luc Van Kaer (Vanderbilt University Medical Center) for support with the experimental research. This study was supported in part by grants from the Japanese Ministry of Education, Culture, Science and Technology, and the Foundation of Osaka Cancer Research, the Ichiro Kanehara Foundation for the Promotion of Medical Science and Medical Care, the Foundation for the Promotion of Cancer Research, the Kanzawa Medical Research Foundation, the Shinshu Medical Foundation, and the Takeda Foundation for Medical Science.

Abbreviations: Ut-LMS, uterine leiomyosarcoma; LMP2, low–molecular-mass polypeptide; IHC, immunohistochemistry; WB, Western blotting; IFN_{γ}, interferon gamma; cdk, cyclin-dependent kinase; STUMP, smooth muscle tumor of uncertain malignant potential; HPF, high-power field; ER, estrogen receptor; PR, progesterone receptor.

Correspondence to: Takuma Hayashi, Dept. of Immunology and Infectious Disease, Shinshu University Graduate School of Medicine, 3-1-1, Asahi, Matsumoto, Nagano 390-8621, Japan.

Tel +81-263-372611;

fax +81-263-372613;

email yoyoyo224@hotmail.com

Received September 8, 2013;

accepted March 13, 2014.

ABSTRACT

Aims and background. Whilst most uterine smooth muscle neoplasms are benign, uterine leiomyosarcoma (Ut-LMS) is extremely malignant with a high incidence of metastasis and recurrence. Gynecological tumors are often associated with female hormone secretion, but no strong link has been detected between human Ut-LMS and the hormonal environment. In fact, the risk factors for Ut-LMS are poorly understood. In addition, no diagnostic biomarkers for differentiating between leiomyoma, a benign tumor, and malignant Ut-LMS have been found. Interestingly, mice that were homozygously deficient for LMP2/β1i were found to spontaneously develop Ut-LMS and exhibited a Ut-LMS prevalence of ~40% by 14 months of age. Thus, analyzing potential risk factors for Ut-LMS (such as LMP2/β1i) might aid the development of diagnostic biomarkers and clinical treatments for the condition.

Methods and study design. Fifty-seven patients (age range: 32-83 years) who had been diagnosed with uterine mesenchymal tumors were chosen from a pathological archive. Tissue samples from these patients were fixed in 10% buffered formalin, incubated in 4% paraformaldehyde for 8 hours, and embedded in paraffin. Tissue sections were stained with hematoxylin and eosin for standard histological examination or were subjected to further processing for immunohistochemical (IHC) examination. Serial Ut-LMS, bizarre leiomyoma, leiomyoma, and myometrium sections were subjected to IHC staining of β-smooth muscle actin, estrogen receptor, cyclin B1, LMP2/β1i, calponin h1, ki-67, tumor protein p53, and progesterone receptor.

Results. The Ut-LMS samples were positive for cyclin B1 and negative for LMP2/β1i, while the opposite result was obtained for bizarre leiomyoma, leiomyoma, and myometrium samples.

Conclusions. The expression pattern of LMP2/β1i and cyclin B1 might be a diagnostic biomarker for human Ut-LMS. Studies of the biological roles of LMP2/β1i and/or cyclin B1 could lead to the elucidation of new targets for therapies against Ut-LMS.

Introduction

The uterus is made up of 3 special layered linings of tissue and muscle. The middle layer is called the myometrium and is also known as the muscular uterine layer. It is composed of smooth muscle which is vital during childbirth to move the baby out of the womb. Uterine mesenchymal tumors, which develop in the myometrium, have been traditionally divided into benign leiomyoma and malignant uterine leiomyosarcoma (Ut-LMS) based on cytological atypia, mitotic activity and other criteria. Ut-LMS is a relatively rare mesenchymal tumor, having an estimated annual incidence of 0.64 per 100,000 women [1]. It accounts for 2% to 5% of tumors of the uterine body and develops more often in the muscle layer of the uterine body than in the cervix. As Ut-LMS is resistant to chemotherapy and radiotherapy, surgical resection, including hysterectomy and bilateral

salpingo-oophorectomy, is the recommended initial treatment strategy[2]. Ut-LMS is an aggressive malignancy, with a 5-year survival of only 35% for tumors confined to the uterus[3,4]. However, the development of an efficient adjuvant therapy is expected to improve the prognosis of Ut-LMS. Leiomyoma may occur in as many as 70%-80% of women by the age of 50 years[5].Distinguishing Ut-LMS from leiomyoma is very difficult, and a diagnosis generally requires surgery and cytoscopy[6]. Diagnostic categories for uterine mesenchymal tumors and morphological criteria are used to assign cases[7,8]. The many different cell lineages of uterine mesenchymal tumors such as the epithelioid and myxoid types are classified in a different way using these features, so the establishment of a diagnostic method is important for the identification of non-standard smooth muscle differentiation.

The molecular mechanisms by which leiomyoma and Ut-LMS develop are not yet known, though tumors that have developed in the myometrium for some reason gradually become larger due to the influence of the female hormone estrogen or a somatic mutation of mediator complex subunit (MED)12[9]. However, no correlation between the development of Ut-LMS and hormonal conditions, and no obvious risk factors for Ut-LMS have been found. Although cases accompanied by hypocalcemia or eosinophilia have been reported, neither clinical abnormality is an initial risk factor for Ut-LMS. The identification of a risk factor associated with the development of Ut-LMS would contribute to the development of preventive and therapeutic strategies.

Cytoplasmic proteins are mostly degraded by a protease complex, which has many substrates consisting of twenty-eight 20- to 30-kDa subunits, referred to as the 20S proteasome[10]. Proteasomal degradation is essential for many cellular processes, including the cell cycle, the regulation of gene expression, and immunological function. Interferon gamma (IFNγ) induces the expression of large numbers of responsive genes, proteasome subunits, i.e. low–molecular-mass polypeptide including LMP2/β1i, LMP7/β5i and LMP10/β2i. A molecular approach to studying the correlation of IFNγ with tumor cell growth has drawn attention[11]. Homozygous mice deficient in LMP2/β1i show tissue- and substrate-dependent abnormalities in the biological functions of the proteasome, and LMP2/β1i correlates with cell survival[12,13]. Ut-LMS occurred in LMP2/β1i-deficient female mice at age 6 months or older, and the incidence at 14 months of age was about 40%[14,15].

Advances in research on the cell cycle have revealed that interaction between cyclins, cyclin-dependent kinases (cdks), and tumor suppressor gene products play essential parts in cell cycle progression[16]. Cyclins, which form complexes with cdks, are a group of proteins periodically expressed during the cell cycle[17]. While normal cells are generally thought to have a normal cell cycle regulatory system, a deranged expression of these cell–cycle-related factors appears to be involved in the malignant transformation of cells[18]. We focused on cyclin B expression patterns in human uterine mesenchymal tumors, because cyclin B plays an integral role in many types of cancer[19-22]. Hyperplasia is one of the hallmarks of cancer. Because cyclin B is necessary for cells to enter mitosis (M) and therefore necessary for cell division, cyclin B levels are often deregulated in tumors. When cyclin B levels are elevated, cells can enter the M phase prematurely and strict control over cell division is lost, which is a favorable condition for cancer development. This being so, the present study was undertaken to investigate the expression of cyclins, especially cyclin B/mitotic cyclin, which is necessary for the progression

of tumor cells into and out of the M phase, in uterine mesenchymal tumors using immunohistochemistry (IHC) and Western blotting (WB). In pathological analyses and WB studies, we identified differential LMP2/β1i and cyclin B1 expression in human uterine mesenchymal tumors. LMP2/β1i and cyclin B1 may be potential diagnostic biomarkers and targeted molecules for a new therapeutic approach.

Material and methods

Tissue collection

A total of 57 patients aged between 32 and 83 years who were diagnosed as having mesenchymal tumors of the uterus were selected from pathological files[23,24]. Serial sections were obtained from at least 2 tissue blocks from each patient for hematoxylin and eosin (HE) staining and IHC studies. All tissues were used with the approval of the ethics committee of Shinshu University after obtaining written consent from each patient.

Leiomyoma variants are classified as benign or malignant based upon histological features. Gross characteristics may suggest that a lesion is benign or malignant, but do not confirm a diagnosis. While some variants include lesions having extrauterine extension or dissemination, this does not automatically confer a diagnosis of malignancy if the histology is benign. On the other hand, some of the variants have histological findings that make it difficult to define them as benign or malignant (e.g. smooth muscle tumors of uncertain malignant potential [STUMP]). Benign smooth muscle tumors (ie, leiomyomas of the usual histological type or "garden-variety" leiomyomas) are defined as follows [7,8,25].

– Low mitotic index (<5 mitoses per 10 high power fields [HPF])
– No cytological atypia
– No cell necrosis (apart from bland degeneration due to tumor ischemia)
– Spindle-shaped cells that are uniform in size and shape
– No intravascular component
– Well-circumscribed mass

Smooth muscle tumors are designated as malignant according to the presence and extent of 3 histological characteristics:

– Abundant mitoses (≥10 per 10 HPF)
– Prominent cellular atypia
– Areas of coagulative tumor cell necrosis in a "geographic" (like islands on a map) fashion

The distinction of leiomyosarcoma from other lesions according to various combinations of these features was proposed based upon a large clinicopathological series (Table 1)[7,8,26].

STUMPs have some characteristics of sarcomas but do not meet the full diagnostic criteria. These tumors are rare and the paucity of data makes it difficult to describe their clinical behavior. It remains to be determined whether STUMP represents a real phenotypic overlap between pathogenetically separate benign and malignant neoplasms. Alternatively, STUMP may represent a true intermediate in a pathway progressing from benign to

malignant. Smooth muscle tumors with features falling just short of satisfying the criteria defined by the largest series also may be malignant [26]. Consequently, atypical smooth muscle tumors with 8 or 9 mitoses per 10 HPFs may be regarded as STUMP, particularly if they have other worrisome features such as atypical mitotic figures or destructive tumor cell infiltration into the smooth muscle fascicles of adjacent myometrium. Smooth muscle tumors with very high mitotic rates (>15 per 10 HPF) also may merit the diagnosis of STUMP due to their rarity and unpredictability.

Table 1 - Classification of problematic uterine smooth muscle tumors based on pathological features

Group	Mitotic index (per 10 HPF)	Atypia	Coagulative tumor cell necrosis	Designation	Meta or recurre
I	≥5 to <20	None or mild	None	Leiomyoma with increased MI	1.
II A	<10	Diffuse, moderate or severe	None	Atypical leiomyoma with low risk percent or recurrence	4.
II B	≥10	Diffuse, moderate or severe	None	Leiomyosarcoma	40
III	≤20	Diffuse, moderate to severe	Present	Leiomyosarcoma	57
IV A	<10	None to mild	Present	Smooth muscle tumors of low malignant potential, limited experience	25
IV B	≥10	None to mild	Present	Leiomyosarcoma	75
V	≥1 to ≤20	Multifocal, moderate to severe	None	Atypical leiomyoma, limited experience	0.

MI, mitotic index; HPF, high-power field.

Immunohistochemistry

IHC staining for LMP2/β1i, calponin h1, estrogen receptor (ER), progesterone receptor (PR), TP53, cyclin B1, α-smooth muscle actin (SMA) and ki-67 was performed on serial human Ut-LMS, bizarre leiomyoma and leiomyoma sections. Antibodies for ER (ER1D5), PR (PR10A), TP53 (DO-1) and ki-67 (MIB-1) were purchased from Immunotech (Marseille, France). The antibody for α-SMA was purchased from Covance Research Products, Inc. (Princeton, NJ, USA). The anti-LMP2/β1i, anti-calponin h1 and anti-cyclin B1 antibodies were produced by SIGMA-Aldrich Israel Ltd. (Rehovot, Israel). IHC was performed using the avidin-biotin complex method as described previously. Briefly, 1 representative 5-μm tissue section was cut from a paraffin-embedded sample of a radical hysterectomy specimen from each patient with Ut-LMS, bizarre leiomyoma and/or leiomyoma. The sections were deparaffinized and rehydrated in graded concentrations of alcohol, incubated with normal mouse serum for 20 minutes, and then incubated at room temperature for 1 hour with primary antibody. Afterwards, sections were incubated with biotinylated secondary antibodies (Dako, Carpinteria, CA, USA) and exposed to a streptavidin complex. The completed reaction was revealed by 3,3¢-diaminobenzidine, and the slide was counterstained with hematoxylin. Normal myometrium portions in the specimens were used as positive controls. Negative controls consisted of tissue sections incubated with normal rabbit IgG instead of the primary antibody. These experiments were registered at Shinshu University in accordance with local guidelines (approval no.

M192). IHC experiments were performed using 6 leiomyoma tissue samples (patients #1, #3, #6, #13, #15 and #21) and 22 leiomyosarcoma tissue samples (patients #1 to #22); the details are shown in Tables 2 and 3. Data were quantified using WinROOF Ver 6.3.0 software (Mitani Co, Ltd, Fukui, Japan). *P* values were generated using a t-test. Data are representative of 3 experiments.

Western blotting

To detect the expression of cyclin B1, LMP2/β1i, LMP7/β5i, calponin h1, α-tubulin and β-actin, whole cell lysates, nuclear extracts or cytosolic extracts were resolved by 10% SDS-PAGE, and WB was performed using appropriate antibodies by standard procedures[23]. The tissue sections from 5 patients (patients #1, #3, #6, #13 and #15) were examined by WB; the details are shown in Tables 2 and 3.

Table 2 - LMP2 and cyclin B1 expression levels in human myometrium, uterine leiomyoma, bizarre leiomyoma a leiomyosarcoma

	Age	n	LMP2 expression				Cyclin B1 expression			
			-	-/+	focal+	+++	-	-/+	focal+	++
Myometrium	32-83	35				35	35			
Leiomyoma	33-83	23				23	23			
Bizarre leiomyoma	44, 49	2				2	2			
Leiomyosarcoma	32-83	32	29	1	1	1			1	31

-/+, partially positive (5% to 10% of cells stained); focal+, focally positive (focal or sporadic staining with less than 5% of cells st diffusely positive (homogeneous distribution with more than 90% of cells stained); -, negative (no stained cells); NA, no answer. *Cyclin B1 expression was examined with the Affymetrix array.

Table 3 - Expression of ER, PR, Ki-67, p53, LMP2/β1i, cyclin B1 and calponin h1 in human uterine leiomyosarcoma

Patient No.	Age (years)	Immunohistochemical staining										Somatic mutations				
		TNM stage	MF	CCN	ER	PR	Ki-67	p53	LMP2	Cy.B	Cal	*TP53*	*JAK1*	*JAK2*	*STAT1*	*LMP2* pro
1	37	T4N1M0	97	+	-	-	3000	+++	-	+++	-	SM	ND	ND	ND	ND
2	58	T3N0M0	24	+	-	-	3500	+	-/+	+++	-	SM	ND	ND	ND	SM
3	45	T2N0M0	32	+	-/+	-/+	2150	+++	-	++	-	SM	M	ND	SM	SM
4	65	T1N0M0	30	+	-/+	-/+	1700	+++	-	+++	-	SM	M	ND	ND	ND
5	52	T1N0M0	107	+	-	+	2600	++	+	+++	-	ND	M	ND	ND	ND
6	49	T1N0M0	46	+	-	-	4300	+	-	+++	-	ND	ND	ND	ND	ND
7	55	T1N0M0	75	+	-	-	4000	+++	-	++	-	ND	ND	ND	SM	SM
8	43	T3N0M0	57	+	+	-	2000	-	-/+	+++	-/+	ND	ND	ND	ND	ND
9	67	T1N0M0	13	+	-	-/+	1430	-	-	+++	-	ND	M	ND	ND	ND
10	67	T1N0M0	37	+	-	-	2100	-	-	+++	-	ND	ND	ND	SM	SM
11	51	T1N0M0	93	+	-	-	4500	-	-	++	-	ND	ND	ND	SM	ND
12	48	T1N0M0	14	+	-	-	900	+++	+	+++	+	ND	ND	ND	ND	ND
13	51	T1N0M0	22	+	-/+	+	450	+	-	+++	-	ND	M	ND	ND	SM
14	67	T1N0M0	64	+	-	+	1450	++	-	+++	-	ND	ND	ND	ND	ND
15	52	T1N0M0	65	+	-	-	1780	++	-	++	-	ND	M	ND	SM	ND
16	42	T3N0M0	73	+	-	-	2130	++	-	+++	-	ND	ND	ND	ND	SM
17	80	T1N0M0	98	+	-	-	1980	+++	-	+++	-	ND	M	ND	ND	ND
18	56	T1N0M0	78	+	-	-	1860	++	-	+++	-	ND	ND	ND	ND	ND
19	58	T1N0M0	40	+	-	-	1750	++	-	+++	-	ND	ND	ND	ND	ND
20	65	T2N0M0	67	+	-	-	780	+++	-	++	-	ND	M	ND	ND	SM
21	45	T1N0M0	52	+	-	-	1045	++	-	+++	-	SM	ND	ND	SM	ND
22	57	T2N0M0	62	+	-	-	980	++	-	+++	-	SM	ND	ND	SM	ND

ER, estrogen receptor; PR, progesterone receptor; Cy.B, cyclin B1; Cal, calponin h1[24,38,39]; SM, somatic mutation; ND, not detected disease; A, alive; MF, mitotic figures/10 high-power fields; CCN, coagulative cell necrosis.

Sequencing of the catalytic domains of the JAK1, JAK2, STAT1 and TP53 genes and the LMP2 promoter region

To determine whether somatic mutations exist in the ATP-binding region or kinase activation domain of *JAK1* and *JAK2*, in the *LMP2/β1i* promoter region, at Tyr701 or Ser727 of *STAT1*, or in the transcriptional activation domain of *TP53* in human Ut-LMS, genomic DNA was isolated and direct sequencing was carried out. Genomic DNA was extracted from consecutive paraffin-embedded Ut-LMS tissue and normal myometrium tissue sections using the microwave-based DNA extraction method for PCR amplification. To avoid contamination of normal myometrium or inflammatory cells, the tumor areas were confirmed using an HE-stained glass slide as a template. The tumor tissues were scraped by razor microdissection from paraffin-embedded consecutive tissue sections. The genomic DNA was subjected to PCR, and restricted DNA fragments for direct sequencing analysis were amplified using published oligonucleotide primers [23-27]. PCR products were directly sequenced using a DYEnamic Terminator Cycle Sequencing Kit (Amersham Biosciences, Piscataway, NJ, USA) with an ABI PRISM 3100 Genetic Analyzer (Applied Biosystems, Foster City, CA, USA).

DNA microarray analysis

The DNA microarray analysis was conducted using tissues extracted from 3 cases of Ut-LMS, 3 cases of uterine leiomyoma and 3 myometrium tissues as described previously[28]. Briefly, from histologically diagnosed tissues, polyadenylated RNA was extracted using an mRNA purification kit (Amersham Biosciences). Affymetrix® GeneChip with Human Genome U133 Plus 2.0 Array was performed in accordance with the manufacturer's recommendations (Affymetrix Ltd., Santa Clara, CA, USA).

Results

In general, it is not easy to distinguish human Ut-LMS from leiomyoma; however, in mice, because of such characteristic pathological findings, significant weight loss, and skeletal muscle metastasis, a tumor that develops in the uterus of an LMP2/β1i-deficient mouse can be considered malignant, i.e. Ut-LMS. The IHC studies with human tissue samples revealed a serious loss in the ability to induce LMP2/β1i expression in human Ut-LMS tissue in comparison with leiomyoma, bizarre leiomyoma or normal myometrium located in the same section. Of the 32 cases of human Ut-LMS that we examined, 29 were negative for LMP2/β1i expression, 1 was completely positive, 1 was focally positive, and 1 was partially positive (Figure 1). Cyclin B1 was a further focus of the present study because of the high ratio of cyclin B1 expression in Ut-LMS compared with leiomyoma, bizarre leiomyoma and myometrium. In IHC studies, all Ut-LMS cases were markedly stained for cyclin B1 (Figure 1 and Table 2). Pathological examination of surgical samples showed the presence of a mass measuring 3 cm in its largest diameter in the lumbar quadrate muscle without a fibrous capsule in general.